Journal of Materials Chemistry B

ROYAL SOCIETY OF CHEMISTRY

PAPER

View Article Online
View Journal

Cite this: DOI: 10.1039/d5tb02873f

Amorphous calcium pyrophosphate bone cement sets without crystallization: a physico-chemical and *in vitro* biological study

L. Touati,[a] M. Y. Hammami,[b] C. Damia,[c] M. Renard,[de] D. Bertrand,[a] M. Durand,[def] J. Amédée,[f] C. Bonhomme[b] and C. Combes *[a]

Calcium phosphate cements have been developed since the 1980s for bone reconstruction. Generally, mixing the solid phase with the liquid phase results in the formation of agglomerated apatite or brushite crystals. This study aimed at formulating the first amorphous calcium phosphate cement constituted of pure amorphous calcium pyrophosphate (a-CPPc: $Ca_2P_2O_7{\cdot}nH_2O$) after setting and hardening at 37 °C in view of developing a bioactive material for bone applications. The amorphous phases involved at each step of the cement preparation were thoroughly characterized using complementary techniques to investigate on the chemical setting reaction. The key role of the structural water content (*n*) and the presence of some orthophosphate ions on the stability of these amorphous phases were evidenced, preventing crystallization but not cement setting and hardening. The acellular *in vitro* study in SBF or TRIS buffer medium including or not alkaline phosphatase enzymes (ALP) showed the bioactivity of this amorphous cement, which remained amorphous after two weeks in SBF solution. In TRIS it transforms into a more stable calcium pyrophosphate crystalline phase and its orthophosphate and calcium ions release is enhanced in presence of ALP. The hydrolysis by ALP of pyrophosphate ions released was demonstrated by phosphate ions titration. The cement cytotoxicity assessment combined with chemical titration allowed optimizing potassium pyrophosphate to be incorporated into the liquid phase (2.5% w/w). Overall, this first set of physico-chemical and biological results on this original biologically responsive a-CPPc cement formulation paves the way to widen the family of bioactive phosphocalcic bone cements with this amorphous hydrated calcium pyrophosphate cement.

Received 22nd December 2025,
Accepted 11th March 2026

DOI: 10.1039/d5tb02873f

rsc.li/materials-b

1. Introduction

Calcium phosphate cements (CPCs) have been developed for more than thirty years and several formulations have reached the market.[1–4] CPCs formulations are mainly constituted of calcium orthophosphates, in some cases associated with other mineral phases such as hydrated calcium sulfate,[5,6] calcium carbonate[7,8] or calcium pyrophosphate[9–11] and/or (bio)polymers.[5,12] Their self-setting reaction leads to the formation mainly of a more or less crystalline hydroxyapatite or brushite phase thanks to a dissolution-crystallization mechanism. Regarding the whole calcium phosphates family, several materials based on calcium pyro- and/or poly-phosphates have been implanted *in vivo* for bone substitution applications.[13–16] Among them, Lee *et al.* have assessed the potential of calcium polyphosphate cement for hard tissue reconstruction and compared it to brushite cements.[16] They showed that polyphosphate cement dissolved much faster (2.5 times) than brushite cement in phosphate buffered saline (PBS) solution at 37 °C. Other authors studied the 3D-printing of polyphosphate cement involving a powder constituted of anhydrous calcium pyrophosphate phase (β-CPP), calcium hydroxide and alginate using water-based binder jetting additive manufacturing but they did not examine the setting reaction.[17] Very recently an original formulation of a crystalline calcium pyrophosphate dihydrate (CPPD) cement has been studied and its physico-chemical and biological bioactivity assessed *in vitro*.[18] Interestingly the *m*-CPPD cement combines a quite high stability in aqueous media even in presence of alkaline phosphatase (ALP) while releasing higher calcium and orthophosphate ions concentration than a biomimetic apatite cement.

[a] CIRIMAT, Toulouse INP, Université de Toulouse, CNRS, ENSIACET, 4 Allée Emile Monso, 31030 Toulouse cedex 4, France. E-mail: christele.combes@ensiacet.fr
[b] LCMCP, UMR 7574, Sorbonne Université, CNRS, Paris, France
[c] Université de Limoges, CNRS, IRCER, UMR 7315, 87000 Limoges, France
[d] CHU de Bordeaux, INSERM, Institut Bergonié, CIC 1401, 33000 Bordeaux, France
[e] Université de Bordeaux, INSERM, Institut Bergonié, CIC 1401, 33000 Bordeaux, France
[f] Université de Bordeaux, INSERM 1026, BioTis, 33076 Bordeaux, France

On the one hand, pyrophosphate ions are known to inhibit calcium phosphate and especially apatite crystallization and dissolution.[19–21] On the other hand, ALP (or other pyrophosphatase enzymes) which are present in living cells are known to hydrolyze the pyrophosphate ions into orthophosphate ions, thus decreasing the mineralization inhibition and favoring apatite formation by increasing orthophosphate concentration locally. So, there is an interest in developing calcium pyrophosphate-based cement as biologically responsive materials thanks to the action of ALP enzymes naturally associated to most living cells. Grover *et al.*[9] studied the effect of the presence of amorphous calcium pyrophosphate in a brushite cement formulated from a mixture of β-TCP, pyrophosphoric acid and orthophosphoric acid. Their *in vivo* results showed that after three months of implantation the cement resorption and bone neoformation were higher than for the non-modified brushite cement (without pyrophosphate). However, these authors did not fully characterize the calcium pyrophosphate amorphous phase which could be responsible for such biological response of the pyrophosphate-modified brushite cement.

Amorphous calcium phosphate materials have gained interest for hard tissue applications due to their bioactivity related to their intrinsic metastability in aqueous media. The latter is of a great biological relevance in dental and skeletal biomineralization and promising as synthetic bone engineering materials.[22–25] The amorphous calcium phosphate phases may be distinguished mainly by the type of phosphate groups associated with calcium, *i.e.* either orthophosphate ions[23] or pyrophosphate ions[26,27] or both.[28–30] The high reactivity of amorphous calcium orthophosphate ($Ca_3(PO_4)_2{\cdot}nH_2O$), known as a precursor of apatite, is supported by its quite fast transformation into biomimetic apatite, *in vitro* and *in vivo*.[31–35] Amorphous calcium pyrophosphate (a-CPP: $Ca_2P_2O_7{\cdot}nH_2O$) shows a high stability for a calcium phosphate amorphous phase[26,27] due to the number of potential conformations related to its P–O–P angle.[26,27,36] As already mentioned above, the ability of pyrophosphate ions to be hydrolyzed into orthophosphate ions *in vitro* and *in vivo* by enzymes such as ALP or in slightly acidic conditions, such as during the few hours or days of inflammation occurring after surgery and/or in pathological conditions, may counterbalance their physicochemical stability.[37–40] Recently Yang *et al.*[41] studied amorphous calcium and magnesium pyrophosphates synthesized by ultrasonic processing in aqueous solution. These authors showed that the amorphous materials obtained were amorphous pyrophosphates associated with orthophosphate ions (about 3–4 times less) probably resulting from the internal pyrophosphate hydrolysis during the ultrasonic synthesis process. The powder prepared with a Mg/Ca molar ratio of 3, with a (Ca + Mg)/P of 1, presented good *in vitro* biological properties in terms of osteogenic differentiation and angiogenic ability associated to a higher release of phosphate and magnesium in SBF. This is the only study demonstrating the bioactivity of pure calcium pyrophosphate amorphous powders materials; the Mg^{2+} ions stabilize and control the bioactive amorphous structure.

Overall, considering the quite high stability of a-CPP phase in aqueous medium, one may consider obtaining this phase through the cement route while avoiding its crystallization and thus maintaining its bioactivity. To the best of our knowledge, there is no a-CPP-based cement and even beyond no CPCs formulation whose final composition is fully constituted of an amorphous phase. Indeed, such a cement route may be counterintuitive for amorphous calcium phosphate cements which setting is in all cases expected to be based on a dissolution crystallization process. Our hypothesis is that developing a formulation of amorphous calcium pyrophosphate self-setting paste could bring several advantages to fit perfectly the bone defect shape and then lead to a cohesive and biologically responsive monolith material after *in vivo* setting. The expected biologically-responsive self-setting material would be related to its composition (fully based on calcium pyrophosphate which should promote ALP enzyme activity) and its bioactivity (its ability to release phosphates and calcium) due to the metastability of the amorphous CPP phase. Development of such strategy and original amorphous calcium pyrophosphate cement material may also widen the range of the well-known phosphocalcic bone cements available to obtain customized materials in terms of resorption and bioactivity.

The objective of this study is to demonstrate for the first time the feasibility to formulate a phosphocalcic cement leading to a fully amorphous calcium pyrophosphate phase after setting and hardening in view of developing a novel design of bioactive and biologically responsive cement for bone filling and repair applications. We developed a self-setting amorphous calcium pyrophosphate cement formulation and assess *in vitro* its cytocompatibility. The amorphous calcium pyrophosphate phases involved at each step of the cement preparation have been fully characterized using complementary techniques (XRD, solid state NMR, TGA). The evolution follow-up of the fully amorphous calcium pyrophosphate set cement was investigated in various aqueous media including or not ALP enzymes to evaluate *in vitro* its bioactivity.

2. Materials and methods

2.1 Reagents

Calcium nitrate tetrahydrate ($Ca(NO_3)_2{\cdot}4H_2O$, Sigma Aldrich, CAS: 13477-34-4, purity: 99.0%) and pyrophosphate precursor salts ($K_4P_2O_7$, Sigma Aldrich, CAS: 7320-34-5, purity: 97% or $Na_4P_2O_7{\cdot}10H_2O$, Sigma Aldrich, CAS: 13472-36-1, purity: 99.5%) were used to prepare the cement reactive powders by double decomposition method in aqueous medium and also incorporated in the cement liquid phase. The solutions used for the a-CPP phase precipitation and for the a-CPP cement (named a-CPPc) formulation were prepared by dissolving the salts in deionized water.

2.2 Synthesis of calcium pyrophosphates powders

The amorphous hydrated calcium pyrophosphate a-CPP ($Ca_2P_2O_7{\cdot}nH_2O$) was synthesized according to a previously

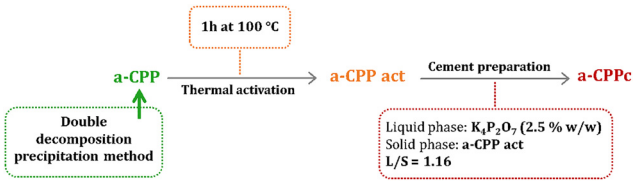

Fig. 1 Simplified diagram of the amorphous material preparation steps involved in the development of the fully amorphous a-CPPc cement formulation: a-CPP, a-CPP act, and a-CPPc.

published protocol.[18] In summary, a calcium nitrate solution was vigorously stirred at room temperature while a potassium pyrophosphate reagent solution was manually and rapidly added to this calcium solution. Once the addition was completed, the resulting precipitate was filtered, washed and then dried in an oven at 37 °C. The as-prepared amorphous phase (a-CPP) was then partially dehydrated (sample called a-CPP act) in a muffle furnace at 100 °C for 60 minutes to enhance its reactivity in the cement formulation (see Fig. 1).

To go further in understanding the role of the number of structural water molecules associated to the starting amorphous powder (a-CPP) in the reactivity of the a-CPP act intermediary powder and then the final a-CPPc cement composition, other drying conditions (duration of the treatment at 37 °C or same drying time but using another drying process: lyophilization) for the precipitated a-CPP was tested.

Also, we synthesized an amorphous calcium pyrophosphate starting powder (called a-CPP P.G) using another protocol[27] (''P.G'' protocol) and then treated and used according to steps summarized in Fig. 1, meaning in the same way as to obtain a-CPP act and a-CPPc from a-CPP precursor powder (Sections 2.2 and 2.3). The a-CPP P.G synthesis protocol differs in terms of calcium concentration and rate at which calcium is added to the pyrophosphate solution: both parameters were lower for a-CPP P.G synthesis than for a-CPP sample; the latter being thus precipitated at higher supersaturation compared to the a-CPP P.G sample.

2.3 Cement preparation

The a-CPPc cement formulation leading to pure amorphous calcium pyrophosphate cement was obtained by mixing manually an appropriate amount of a-CPP act powder with an aqueous solution of $K_4P_2O_7$ (in deionized water) used as cement liquid phase and also setting accelerator (Fig. 1). The composition of the cement powder and liquid phase is reported in Table 1. The paste was then molded into a silicone mold (cylindrical disk of 9 mm in diameter and 2 mm thick) and put in an oven at 37 °C for 24 hours to set and harden in a water-saturated atmosphere, and finally dried in air.

Table 1 Solid and liquid phase composition for a-CPPc cement formulation

Solid phase		Liquid phase		L/S
CPP phase	Mass (g)	Composition	Mass (g)	(w/w)
Thermally activated a-CPP (a-CPP act)	0.60	2.5% w/w $K_4P_2O_7$	0.70	1.16

2.4 Characterization of amorphous powders and cement

The a-CPP and a-CPP act reactive powders and a-CPPc cement (before and after *in vitro* tests) were systematically characterized by X-ray diffraction (XRD), Fourier transform infrared (FTIR) spectroscopy and scanning electron microscopy (SEM). To go further chemical analysis, Raman spectroscopy and solid-state NMR were also performed. The physical characteristics of a-CPPc cement were also investigated.

Powders and materials were observed by SEM (FEI Quanta 450 microscope), in low vacuum mode. All samples were stuck onto double-sided carbon tape before their observation. XRD analyses were performed using a Bruker D8 diffractometer, with a copper anticathode K_α, λ_{Cu} = 1.5418 Å. Complementary structural information was obtained by FTIR spectroscopy using a Thermo Electron Nicolet iS50 spectrometer in transmission mode (KBr pellet) with 64 scans at a resolution of 4 cm^{-1}.

Calcium and phosphorus (orthophosphate and pyrophosphate ions) in amorphous samples (a-CPP, a-CPP act and a-CPPc) were titrated in triplicate using a complexometric method with EDTA and visible spectrophotometry at λ = 460 nm (using Shimadzu UV1800 spectrophotometer) of yellow coloration of phospho-vanadomolybdenum complex in acidic solution, respectively and as described previously.[18,29]

Thermogravimetric analyses (TGA) and differential thermal analyses (DTA) were performed with a Setsys Evolution System (Setaram) instrument in the temperature range from 25 to 500 °C with a heating rate of 5 °C per minute in airflow. The measurements were performed in triplicate and the uncertainty in the measurement is 0.2%. The standard deviation (SD) on the number of structural water molecules determined from these measurements has been evaluated. Also, the significance of the differences between these results was assessed by performing a ''Two sample *t*-test'' using Origin software after having checked normality of values distribution (''Normality test''). *P* values < 0.05 were considered statistically significant.

Raman spectroscopy analyses were carried out using a Raman confocal microscope, Labram HR 800 Horiba Yvon Jobin with a 532 nm argon diode laser and a cooled CCD Synapse quantum detector. To provide a representative analysis of sample, each analysis was performed three times in a single point (lateral resolution = 0.72 µm, axial resolution = 2.63 µm).

^1H and ^{31}P NMR data were collected on a Bruker Avance NEO solid-state NMR spectrometer operating at a magnetic field of 16.44 T (standard bore magnet) using a 4 mm H/X probe at a spinning frequency of 14 kHz. The resonance frequency of ^1H and ^{31}P were 699.68 MHz and 283.23 MHz respectively. ^1H MAS NMR spectra were acquired using a composite pulse sequence to filter background signal before acquisition, with a 90° pulse duration of 4.2 µs, a recycle delay of 5 s, and a number of scans of 8.

^1H–^{31}P cross-polarization (CP) MAS NMR spectra were performed using a contact time of 3 ms. A pre-saturation was applied systematically on ^{31}P channel to eliminate direct

Zeeman contributions. The recycle delay is set at 5 s, number of scans at 512. Spinal64 is used as ^{1}H–^{31}P decoupling scheme.[42]

All chemical shifts were referenced indirectly using ^{31}P NMR (H_3PO_4) frequency and xiref referencing. All equipment used for filling rotors were cleaned with ethanol and dried after each experiment. Cement samples were slightly crushed to ensure better homogeneity of rotor filling. Spectra were treated using the ssNake program (https://github.com/smeerten/ssnake).

The cement sample porosity was determined by mercury intrusion porometry (Micromeritics Auto Pore 9510 porosimeter, uncertainty on measurement: 1 to 1.5%). The initial and final setting time of the cement paste was evaluated using the Gillmore Needles standard method (ASTM-C266-89).

2.5 Follow-up of the a-CPPc cement paste setting chemical reaction

The setting chemical reaction of the a-CPPc cement paste was monitored by XRD, SEM and FTIR spectroscopy after several maturation times at 37 °C and in wet atmosphere: 0, 20 min, 1 h, 6 h, 24 h, 48 h, 72 h and 7 days. The protocol has been previously published.[18] Briefly, at each selected time point the paste was subjected to quenching in liquid nitrogen, followed by lyophilization to stop the setting chemical reaction, and then characterized.

The characterization of the samples was found to be reproducible; consequently, only one of the triplicate samples characterized is presented in the figures. The time referred as "t_0" corresponds to the cement solid phase (*i.e.* a-CPP act) before the liquid phase was added.

2.6 Evolution study of the set and dried cement in different aqueous media

The physico-chemical evolution of set and dried fully amorphous a-CPPc cement material (prepared as described in Section 2.3) in three types of aqueous media was investigated. Three aqueous media (SBF, TRIS buffer and TRIS buffer + ALP enzyme) were tested; protocols for preparing these three different aqueous media has already been described.[18,29] SBF solution which simulates the inorganic ions composition of the blood plasma and includes tris(hydroxymethyl)aminomethane (TRIS, VWR, CAS 77-86-1, purity ≥ 99%) buffer to stabilize the pH of the solution at 7.4, TRIS buffer solution and a TRIS buffer solution including alkaline phosphatase enzymes (Alkaline phosphatase from bovine intestinal mucosa, Sigma Aldrich, CAS: 9001-78-9, medium named TRIS + ALP). The pH of the latter being set at 8.1 for optimized ALP enzyme activity. The goal of the study, pH and time points investigated for each experiment in specific type of medium are summarized in Table 2.

a-CPPc cement disk (about 100 mg, "Initial disk") was immersed in the prepared solution (100 mL of SBF, TRIS or TRIS + ALP solution), in a tightly closed container and placed in a bath at 37 °C and under low magnetic stirring. Experiments were performed in triplicate for each time point and each aqueous medium. For each time point selected, a-CPPc cements were removed from the solution, rinsed in deionized water and ethanol bath, dried at room temperature and finally the disks were weighed and characterized. Solutions were filtered on a 0.45 μm cellulose porous membrane before pH measurement and chemical titration.

Table 2 pH and selected time points for the study of the a-CPPc cement evolution in the different aqueous media at 37 °C

Aqueous media	Goal of the study	pH	Evolution times
SBF	Testing cement's bioactivity	7.4	7 h; 2, 7 and 15 days
TRIS TRIS + ALP	Effect of ALP enzymes on bioactivity of a-CPPc cement	8.1	2 and 6 days

To investigate the possible chemical and structural composition evolution of the a-CPPc cement, samples were analyzed by XRD, FTIR spectroscopy and SEM as mentioned in Section 2.4. The mass loss of the a-CPPc cement was also evaluated.

Titration of calcium and phosphate ions (orthophosphate and pyrophosphate ions) in the medium after cement immersion has been achieved for each selected contact time point. The titration methods have been described in the literature:[18,29] Ca^{2+} titration was carried out by atomic absorption spectrometry (AAS, Thermo Scientific ICE 3000 spectrometer; Waltham, MA, USA). Orthophosphate ions (PO_4^{3-} or HPO_4^{2-}) were titrated by visible spectrophotometry (as described in Section 2.4). Finally, $P_2O_7^{4-}$ ions released were titrated using a commercial kit, PPI Light kit (Lonza), and using a luminometer (Berthold, Junior luminometer LB 9509). The pH of the medium was measured at each time point.

To check the significance of the differences between the results we performed a "Two sample *t*-test" using Origin software after having checked normality of values distribution ("Normality test"). *P* values < 0.05 were considered statistically significant.

2.7 Cement *in vitro* biological assessment

Cement disks were sterilized by γ-ray (25 KGy) or UV irradiation (BLX-254 Bio-Link UV irradiation system, 1 hour) before the cell culture assays.

The MTT (methylthiazolyldiphenyl tetrazolium bromide) assay is a quantitative colorimetric measure of cell viability (ISO 10993-5). The method has already been described.[43] a-CPPc cement disks were prepared from a liquid phase containing 2.5% w/w or 5% w/w $K_4P_2O_7$. These disks were incubated for 48 hours (37 °C, 60 rpm) at 3 cm^2 mL^{-1} in serum-free culture medium (Eagle's minimum essential medium (EMEM), ATCC). After 48 hours, the extracts showed microparticles incompatible with this test on clear extract solutions (no particle in suspension), so the extracts were centrifuged (12 000*g* for 10 min) and then filtered at 0.2 μm. The filtered extracts were finally supplemented with 10% horse serum, then dilutions were made in 10% serum medium to obtain 4 concentrations: 100%, 50%, 10% and 1%. Only the pure extract (100%) is considered for cytotoxicity; other dilutions allow us to understand the severity of cytotoxicity. Thermanox™ coverslip was used as negative control, while latex-based biomaterial was used as positive control.

L929 cells (Fibroblast cell line, CCL1 (ATCC)) were cultured in EMEM medium (ATCC) supplemented with 10% (v/v) of horse serum (bio sera). Cells, seeded at 3.3×10^4 cm^{-2} in 96 wells (0.31 cm^2 wells), were cultured 24 hours before depositing the extracts and then cultured in the presence of the extracts for 24 h before the MTT assay. The supernatant was removed (and stored for later experiments of potassium ions titration) and cells were rinsed with PBS. Living cells transform tetrazolium salts (CAS 298-93-1, yellow in color) into formazan crystals (insoluble in aqueous media, blue-violet in color). The viable cell count corresponds to the color intensity determined by photometric measurements after dissolution of the formazan. The cells were incubated for two hours at 37 °C, 5% CO_2, in a wet atmosphere in the presence of 1 mg mL^{-1} of tetrazolium salt in culture medium without phenol red or serum. At the end of the incubation period, the reagent is decanted, and the formazan crystals present in the cells were then solubilized using DMSO and the absorbance read at 550 nm.

Potassium ions concentration in extracts, supernatants and medium (EMEM + 10% v/v serum) samples were titrated by atomic absorption spectrometry (AAS, Thermo Scientific ICE 3000, Waltham, MA, USA). Each sample solution analyzed was acidified by adding 1% v/v of nitric acid (HNO_3 at 69%, 1.01799, No. CAS: 7697-37-2, VWR), and also 0.5% v/v of $LaCl_3$ (Cat. 140-003-421, SCP SCIENCE) and 0.5% v/v of CsCl (Cat. 140-003-241, SCP SCIENCE) as matrix modifiers in order to enhance the titration of potassium and overcome interference related to the presence of phosphate ions in the solutions. The wavelength for potassium ion analysis is 766.5 nm and the calibration line was [0.5, 0.75, 1, 1.25, 1.5 and 1.75 ppm] prepared in identical experimental conditions from a potassium standard solution (1000 ppm; Cat. 140-001-191, SCP SCIENCE).

3. Results and discussion

3.1 Physico-chemical characterization of the amorphous powders and a-CPPc cement

3.1.1 Study of the a-CPPc cement paste maturation and setting. As already demonstrated in a previous study,[18] characterization of the a-CPP and a-CPP act phases by XRD, FTIR spectroscopy and SEM confirmed that the amorphous nature of the a-CPP phase is maintained after heat treatment.[26] A more thorough analysis of possible structural changes that occurred between a-CPP and a-CPP act samples is presented later in this article.

After a preliminary test showing the feasibility of this self-setting paste prepared from a-CPP act reactive powder, Fig. 2 and 3 illustrate the XRD and SEM monitoring of the physico-chemical evolution of the a-CPPc cement paste during its maturation in a wet environment at 37 °C. The composition of the cement is homogeneous and the amorphous structure maintained up to 48 hours as presented on XRD analysis (Fig. 2). A significant increase of the proportion of a crystalline phase, identified as calcium pyrophosphate dihydrate (*m*-CPPD: $Ca_2P_2O_7{\cdot}2H_2O$), was observed after a maturation period of 7 days.

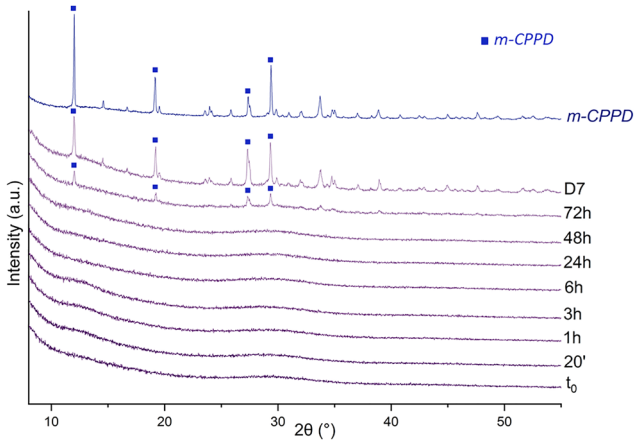

Fig. 2 Focus in 5–55° (2θ) domain of XRD diffractograms of the a-CPPc cement paste during its maturation, *i.e.* setting and hardening, between t_0 to 7 days (t_0 constitutes the point before addition of the liquid phase to the dried a-CPP act powder). The square legends indicate the four main peaks selected to illustrate the presence of the *m*-CPPD phase in the cement paste.

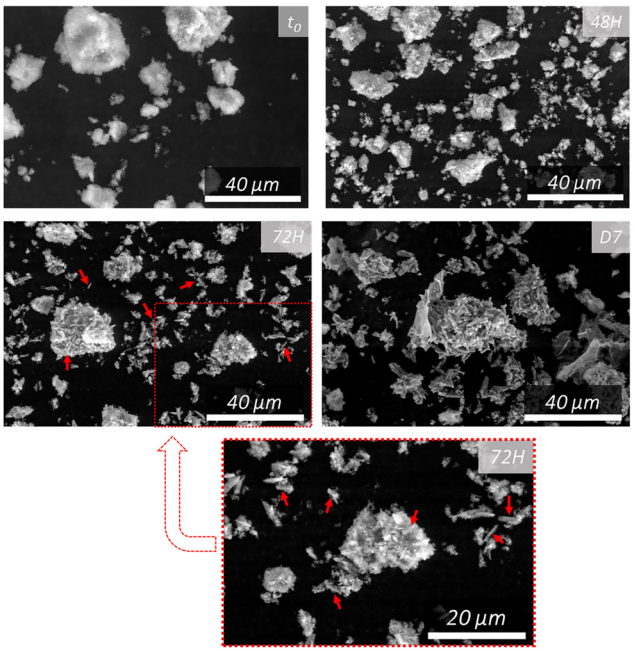

Fig. 3 SEM images of a-CPPc cement paste during setting and hardening, between t_0 and 7 days (t_0 corresponds to the dried a-CPP act powder, before addition of the liquid phase). Red arrows indicate some of the *m*-CPPD crystals in the sample.

FTIR spectroscopy (Fig. S1) and SEM analysis (Fig. 3) confirm the presence of an amorphous phase of calcium pyrophosphate in form of agglomerates for up to 48 hours. However, after one week of maturation, the main phase is found to be the *m*-CPPD crystalline phase showing the characteristic needle shape crystals. Interestingly, the a-CPPc cement presents no significant structural change during 48 hours of maturation time even though mechanical consolidation occurs during this stage: a-CPPc cement remains fully amorphous at least up to 48 h of maturation while

its initial and final setting time measured using the Gillmore needles method were 22 ± 2 and 270 ± 10 minutes, respectively. For the rest of the study a-CPPc cement corresponds to a fully amorphous calcium pyrophosphate hard and cohesive cement (see XRD on Fig. S2a) obtained after 24 hours of maturation time (37 °C, wet atmosphere) and dried during 24 hours in the oven (37 °C) as mentioned in Section 2.3. This a-CPPc cement showed a high porosity (70%), its porogram is presented on Fig. S2b.

3.1.2 Comparison of the various amorphous calcium pyrophosphate phases involved from the a-CPP precursor powder to the set a-CPPc cement. The chemical composition (calcium and phosphate) in the amorphous materials (a-CPP, a-CPP act and a-CPPc cement after 24 hours of maturation and drying at 37 °C) is reported in Table 3. The results show that the proportion of phosphorus in the form of orthophosphate ions (PO_4^{3-} or HPO_4^{2-}) in the a-CPP act and a-CPPc samples is higher than in the a-CPP samples. Orthophosphate ions have been identified in the literature as a stabilizing agent of amorphous mineral phases, and in particular they are known to inhibit the crystallization of CPP phases.[21,26,44] As expected, the difference between the Ca/P obtained for a-CPP and a-CPP act powders was found to be non-significant considering the standard deviation on these Ca/P values. The Ca/P ratio obtained for the a-CPPc cement should be lower than that expected for the CPP phases, *i.e.* Ca/P = 1. Indeed, considering all the Ca and P introduced initially in the a-CPPc formulation (Table 1), the calculated Ca/P is 0.97 (lower than 1) due to the contribution of pyrophosphate ions also introduced *via* the liquid phase ($K_4P_2O_7$ salt dissolved). The latter leads to an excess of P content (as pyro- and ortho-phosphates, see Table 3) as compare to that of a-CPP act powder, which decreases the Ca/P ratio for the a-CPPc samples. The experimental value obtained from chemical analyses results (Table 3) is slightly lower (0.86 ± 0.06).

TGA analyses of these amorphous samples (a-CPP, a-CPP act and a-CPPc after 24 hours of maturation and drying at 37 °C) point out a one-step mass loss for all samples (Fig. S3), in agreement with the literature.[27] Table 4 summarizes the number of water molecules associated to each amorphous sample, as-determined by TGA analysis. The precipitated a-CPP phase dried at 37 °C has 3.68 water molecules, which is consistent with the description proposed in the literature (number of structural water molecules (n) ranging from 3.8 to 4.2).[26,36] Thermal activation of this phase leading to a-CPP act powder reduces the water content to 2.25 molecules. The a-CPPc cement prepared from the latter includes 2.72 water molecules. It therefore appears that during cement setting, the paste formed by mixing the solid phase with the liquid phase hydrates slightly. However, in the end the a-CPPc cement has a structural water content (n = 2.72) that is closer to that of the *m*-CPPD phase ($Ca_2P_2O_7{\cdot}2H_2O$) compared to the initial a-CPP powder (n = 3.68).

Table 3 Calcium and phosphorus as $P_2O_7^{4-}$, PO_4^{3-} and HPO_4^{2-} ions contents (and the related Ca/P atomic ratio) in a-CPP and a-CPP act powders and a-CPPc cement, determined by chemical analyses

Samples	P: $P_2O_7^{4-}$ (%w)	P: PO_4^{3-} or HPO_4^{2-} (%w)	Ca^{2+} (%w)	Ca/P
a-CPP	16.8 ± 0.2	0.68 ± 0.04	21.9 ± 0.7	0.97 ± 0.06
a-CPP act	16.1 ± 0.1	1.38 ± 0.04	24.9 ± 0.8	1.10 ± 0.09
a-CPPc	17.9 ± 0.3	1.43 ± 0.08	21.5 ± 0.7	0.86 ± 0.06

Table 4 Number of structural water molecules determined by TGA analyses for a-CPP, a-CPP act and a-CPPc amorphous materials, $Ca_2P_2O_7{\cdot}nH_2O$

Sample	Mass loss (%w)	Average number of water molecules (n) per $Ca_2P_2O_7$ (±SD)
a-CPP	20.7	3.68 ± 0.05
a-CPP act (thermal activation)	13.8	2.25 ± 0.05
a-CPPc (after 48 h of maturation time)	15.8	2.72 ± 0.06

The environment of phosphorus within a-CPP, a-CPP act, and a-CPPc samples was further investigated using solid state NMR spectroscopy. The objective is to identify the influence of each stage of cement production (illustrated in Fig. 1) on the organization of amorphous materials obtained. Fig. 4 presents the ^{1}H MAS and ^{1}H–^{31}P CP MAS spectra of the three types of amorphous samples prepared according to protocols presented in Fig. 1. The isotropic chemical shifts of the ^{1}H or ^{31}P are summarized in Table S1. A simulation of the NMR spectra was performed using ssNake software to support the analysis of the spectra obtained (Fig. S4).

The amorphous samples exhibit two distinct environments around 5 ppm and between 0 ppm and 4 ppm (Fig. 4A). It can be seen that the a-CPP peak is broader than that of the a-CPP act, indicating a potential increase in the organization of H-bond network induced by the thermal activation step (a-CPP act sample). In agreement with the work of Gras *et al.*,[36] the resonance around 5 ppm corresponds to weakly bound water molecules (but nevertheless in H-bond networks). Within a-CPPc, this peak widens further, which could correspond to a less organized phase. Peaks between 0 ppm and 2 ppm are similar to those associated with biomimetic apatite samples; more specifically, the peak at 0.20 ppm could correspond to OH^- ions.[45] However, these low-intensity peaks represent less than 1% of the spectrum (according to the simulation in Fig. S4) and their interpretation is delicate and debatable. By the way, hydroxyapatite is not detected by powder XRD meaning that its amount is indeed extremely small. The peaks at 1.24 and 3.83 ppm may correspond to some residues of ethanol which was used to wash the rotor.

The ^{1}H–^{31}P CP MAS NMR spectra displays a major, broad component centered around −7 ppm, associated with pyrophosphate species as identified by Slater *et al.*[26] and Gras *et al.*[36] A more or less pronounced shoulder is observed between 0 and 8 ppm, its intensity increasing after activation of the samples (yellow band in Fig. 4B). We checked the significance of the differences observed between NMR spectra of a-CPP and a-CPP act powders (Fig. 4C.1) and a-CPP and a-CPPc (Fig. 4C.2). We can see that the difference between the spectra (1 and 2) is well over the noise. It should be noted that each spectrum has been treated in the same way (same chemical shifts

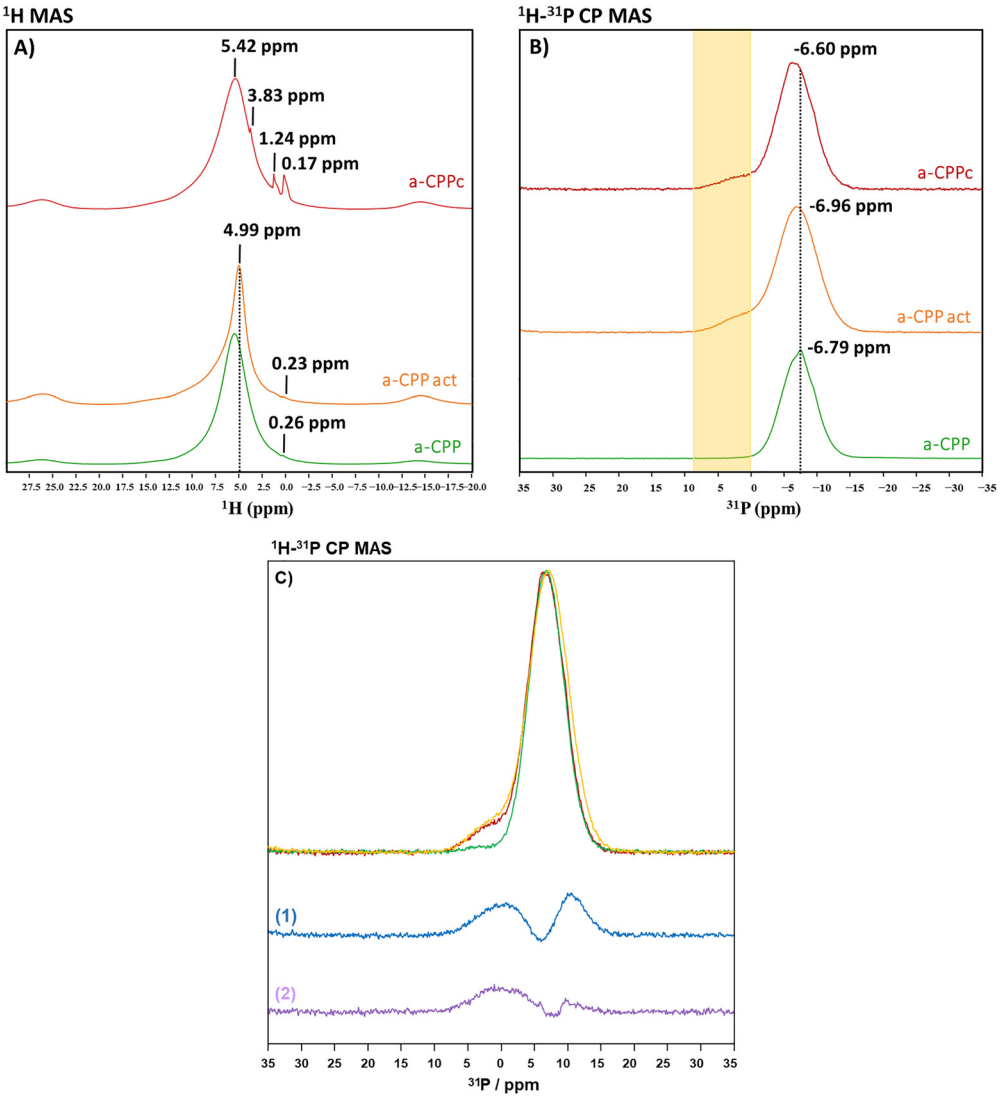

Fig. 4 ^{1}H (A) and ^{1}H–^{31}P CP MAS (B) NMR spectra obtained for an a-CPP sample, as well as for the associated a-CPP act and a-CPPc samples. (C) Overlapped ^{1}H–^{31}P CP MAS NMR spectra obtained for a-CPP (green), a-CPP act (orange) and a-CPPc (red) samples as presented in B: (1) corresponds to the subtraction between a-CPP and a-CPP act spectra; (2) corresponds to the subtraction between a-CPP and a-CPPc spectra.

reference, same phase). We can clearly see that it is at the final step (a-CPPc cement) that a slightly more pronounced difference between spectra (2) is affecting the main contribution of the signal. In both cases (1,2), the appearance of a shoulder at higher chemical shift is observed. This shoulder corresponds to orthophosphate ions (PO_4^{3-}, HPO_4^{2-}) as suggested by the work of Slater *et al.*[26] and Gras *et al.*[36] which is confirmed by the phosphorus titration presented in Table 3. However, in ^{1}H NMR, the contribution of HPO_4^{2-} ions is hardly visible, which leads us to believe that these environments of phosphorus are assigned to PO_4^{3-} species. In addition, ^{31}P MAS and CP MAS spectra are comparable meaning that PO_4^{3-} species are mainly present. These observations contradict those observed by Slater *et al.*,[26] who had identified the formation of HPO_4^{2-} ions.

To go further in the interpretation of NMR results and refine materials characterization, it would be interesting to perform 2D ^{1}H–^{31}P CP MAS experiments with low contact time. The presence of any correlation patterns would directly highlight the proximity of the ^{31}P and ^{1}H nuclei of the POH groups within the HPO_4^{2-} ions.

3.1.3 Discussion on a-CPPc stability and reactivity. The more refined characterization of the various amorphous samples: a-CPP and a-CPP act (starting reagents) and final a-CPPc cement using ^{1}H MAS and ^{1}H–^{31}P CP NMR spectroscopy does not reveal significant changes in the organization of the water molecules in the synthesized a-CPP sample and the resulting a-CPPc cement (Fig. 4). To go further an a-CPPc cement was also prepared from an amorphous a-CPP starting powder synthesized using the protocol developed by Gras *et al.*[27] (called a-CPP P.G) and then treated and used in the same way as a-CPP sample synthesized as described in Section 2.2 and according to steps summarized in Fig. 1 (a-CPP act and a-CPPc). As indicated in Section 2.2, the a-CPP P.G synthesis protocol

differs from a-CPP protocol in terms of supersaturation: a-CPP precipitated at higher supersaturation condition compared to a-CPP P.G. The ^{1}H MAS and ^{1}H–^{31}P CP NMR spectra (Fig. S5 and Table S2) show that a-CPP ''P.G'' protocol leads to the formation of amorphous materials a-CPP P.G and its related a-CPP act and a-CPPc with additional ^{1}H environments. This result indicates that hydrogen bond network of water molecules within the a-CPP and a-CPP act phases depends on the synthesis protocol used for the amorphous calcium pyrophosphate starting powder (a-CPP or a-CPP P.G), and this structure is preserved within the corresponding a-CPPc cement.

^{31}P NMR (Fig. 4) and chemical analysis (Table 3) of amorphous samples revealed the presence of orthophosphate ions. Both techniques agree that the proportion of orthophosphate is higher in the corresponding a-CPP act and a-CPPc cement samples compared to the initial a-CPP precipitated powder (a-CPP, a-CPP act and a-CPPc as presented in Fig. 1). In the case of thermally activated a-CPP (a-CPP act), previous work has demonstrated that heat treatment (140–220 °C) can promote the internal hydrolysis of pyrophosphate ions to form orthophosphate ions according to the following equations:[26]

$$P_2O_7^{4-} + H_2O \rightarrow 2\ HPO_4^{2-} \quad (1)$$

$$HPO_4^{2-} + H_2O \leftrightarrow PO_4^{3-} + H_3O^{+} \quad (2)$$

The presence and subsequent increase of orthophosphate ions formed during the thermal activation step contribute to the stabilization of a-CPP act amorphous sample, while the loss of structural water molecules associated with this amorphous phase (Table 2) contributes to its reactivity. The work of Slater *et al.*[26] has also demonstrated the spontaneous nature of the hydrolysis reaction of pyrophosphate ions within the amorphous a-CPP phase (equations 1 and 2). It appears that the present cement route is associated with the formation of orthophosphate ions *via* various hydrolysis processes: the internal hydrolysis of pyrophosphate ions induced by the thermal activation of the amorphous reactive powder (a-CPP act) and the one intrinsically related to the amorphous nature/reactivity of such hydrated amorphous phases (a-CPP and a-CPP act). Indeed, the stabilizing role of these orthophosphate ions has been identified in the literature, as they inhibit the crystallization of calcium pyrophosphate.[19,21,44,46]

TGA analyses have shown that a-CPPc cement consists of a number of structural water molecules closer to the a-CPP act phase (approximately 2.2) than to the initial a-CPP (3.7). It consists of approximately 2.6 water molecules closer to the dihydrate calcium pyrophosphate m-CPPD. This observation is consistent with the partial crystallization of the a-CPPc paste into *m*-CPPD phase identified from 72 hours of maturation at 37 °C in a wet environment (Fig. 2). The crystallization of a-CPP after 7 days of immersion in acidic water at pH 5.8 and 50 °C was also reported.[47] In order to further evaluate the influence of structural water molecules in the a-CPP act reactive phase on the structure and crystallization of a-CPPc cement paste, the latter was prepared using three different a-CPP act powders. Indeed, the a-CPP starting phase was dried using three different methods: dried in oven at 37 °C during 16 h or over 24 h or lyophilized during 16 h (Table 5). Then it should be noted that the protocol of thermal activation (a-CPP act) of these three a-CPP samples was strictly identical (a-CPP act obtained after 1 hour at 100 °C). Also, the three related a-CPPc cements were dried after 7 days of maturation time (wet atmosphere, 37 °C) to ensure with such a long maturation time that any potential crystallization of the amorphous cement towards a crystalline phase could be observed (Table 5).

The water content in the reactive a-CPP act phase varies between 1.57 and 3.36 water molecules per $Ca_2P_2O_7$ unit (see TGA curves of the three a-CPP act in Fig. S6.A), whereas the a-CPPc cement obtained contains a maximum of 2.5 water molecules, and a minimum of 2.1 molecules. The case of a-CPPc sample no. 1 is noteworthy, as it has the lowest number of water molecules per $Ca_2P_2O_7$ unit (n = 2.1) and is very close to that of the *m*-CPPD dihydrated phase. Furthermore, after 7 days of maturation, it is the only cement sample for which crystallization towards the *m*-CPPD phase (see X-ray diffractograms of the three a-CPPc cements in Fig. S6.B) has been observed while it was obtained from the a-CPP act sample with the highest water molecule content tested (n = 3.36).

The structure and number of water molecules per $Ca_2P_2O_7$ unit present in a-CPP reactive powder (a-CPP act) appear to influence both the organization of the final hydrogen network of the cement obtained and the stability of its amorphous structure. The crucial role of the number of structural water molecules is also known to stabilize other amorphous mineral phases as amorphous calcium carbonate.[48,49] This is the first phosphocalcic cement formulation that result in cohesive and fully amorphous cement composition after setting and hardening. This raises the question of the mechanism responsible for setting of such a-CPPc cement compared to the well-known CPC cements, which setting and hardening is associated to the entanglement of crystals of the more stable crystalline phase that is formed during setting and hardening.

Table 5 Average number of structural water molecules (n) per $Ca_2P_2O_7$ unit ($Ca_2P_2O_7{\cdot}nH_2O$) determined by TGA analyses of the a-CPP dried using three different protocols, and their related a-CPP act and a-CPPc amorphous calcium pyrophosphate phases

a-CPPc cement (after 7 days of maturation time)	a-CPP drying protocol	n of a-CPP act (±0.03)	n of a-CPPc (±0.03)	Composition of the set a-CPPc cement
1	37 °C during 16 h	3.36	2.10	*m*-CPPD + a-CPP
2	37 °C during > 24 h	2.25	2.27	a-CPP
3	Lyophilization during 16 h	1.57	2.48	a-CPP

3.2 Study of the set and dried a-CPPc cement evolution in different aqueous media

3.2.1 Evolution in SBF solution. The XRD patterns of the a-CPPc cement before and after immersion in SBF points out the beginning of the crystallization of the amorphous a-CPP phase into *m*-CPPD phase after 2 days of immersion in the SBF solution (Fig. 5). Indeed, from day 2 some peaks of very low intensity may be slightly distinguished from $2\theta = 25^\circ$ to 30° on the diffuse halo but their relative intensity did not increase significantly with time thereafter, the amorphous phase remaining in great majority (Fig. 5). The vibrational signatures of the amorphous CPP phase were revealed also by FTIR and Raman spectroscopy (Fig. S7). In addition, after 7 and 15 days of immersion in SBF medium, Raman spectra of a-CPPc exhibited a band at 955 cm^{-1}, which demonstrates an increased intensity after 15 days. This band can be assigned to $\nu^{s}PO_4$ of orthophosphate ions which are observed in apatite structure (see Fig. S7). The SEM images (Fig. 6) illustrate the formation on the surface of the cement of needle-shaped crystals characteristic of the *m*-CPPD phase, which was identified by XRD analyses to contribute in very low amount (Fig. 5). Finally, cracks are clearly observed on the surface of the a-CPPc cement at day 7 and 15 (Fig. 6). These cracks may be due to the drying of the disk (after its evolution in solution and before its observation by SEM) provoking a shrinkage during water elimination from the sample surface, and/or to the degradation of the material itself in the aqueous medium.

The mass loss values of a-CPPc cement disk as function of its time of immersion in SBF solution are reported in Table 6. The difference in mass loss is very low in all cases. Indeed, the statistical test did not reveal significant difference between the values corresponding to a different immersion time. However, a slight tendency to an increase may appear at 2 to 7 day coinciding with the beginning of the crystallization of the *m*-CPPD phase identified by XRD (Fig. 5) and observed on cement disk surface by SEM (Fig. 6).

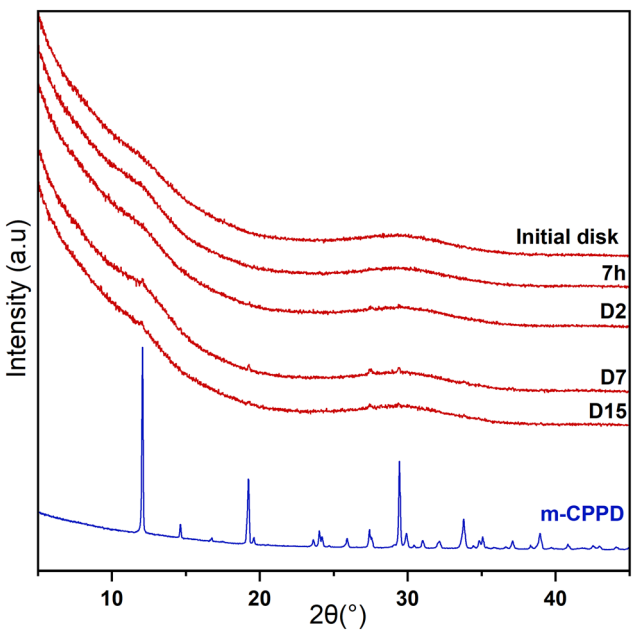

Fig. 5 XRD diffractograms of a-CPPc cement before (initial disk) and after its immersion during 7 h, 2, 7 and 15 days in SBF solution.

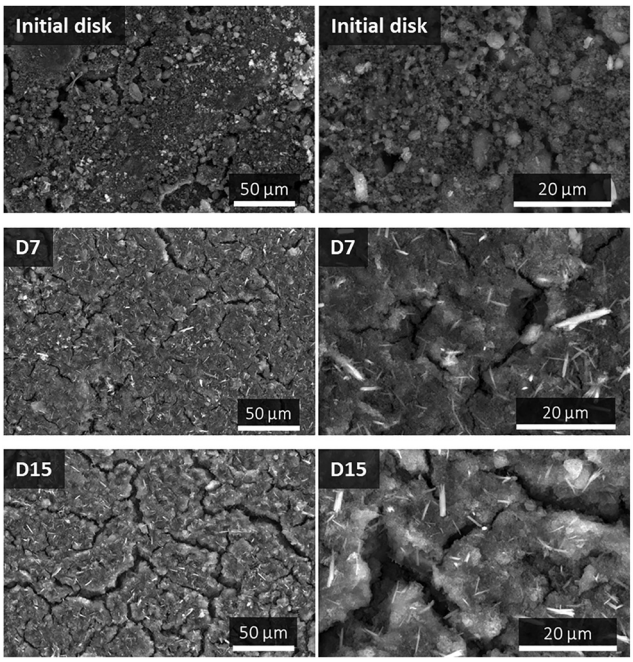

Fig. 6 SEM images at different magnifications of a-CPPc disk surface before and after 7 and 15 days of immersion in SBF solution.

Table 6 Evolution of a-CPPc cement disk mass after different periods of immersion in SBF solution. The value is expressed as a percentage of the initial mass of the cement disk (tests realized in triplicate)

Immersion time	Δm (%)	Standard deviation (%)
7 h	−9	2
D2	−13	6
D7	−11	1
D15	−6	1

The titration of the solutions collected after cement material immersion in SBF solution and their pH evolution are presented in Fig. 7. These results showed an early release of calcium and pyrophosphate ions associated with a fast decrease of the pH down to nearly acidic pH. After 2 days of a-CPPc immersion, the pH decreased rapidly down to 6.2 and then increased up to neutral pH at day 7 to finally reached a pH close to 8 after 15 days.

The maximum concentrations of calcium and pyrophosphate ions detected in SBF medium are 2.9 mM and 0.13 mM, respectively after 7 days of immersion. Then, these concentrations decrease, following a Ca/Pyro ratio around 2.5, down to 2.8 mM and 0.09 mM at 15 days of immersion. These variations in concentration and ratio are consistent with the precipitation of the *m*-CPPD phase (Ca/Pyro = 2) as a slight crystallization of a-CPPc into *m*-CPPD was identified by XRD (Fig. 5) and SEM (Fig. 6) from 7 days of immersion. The concentration of

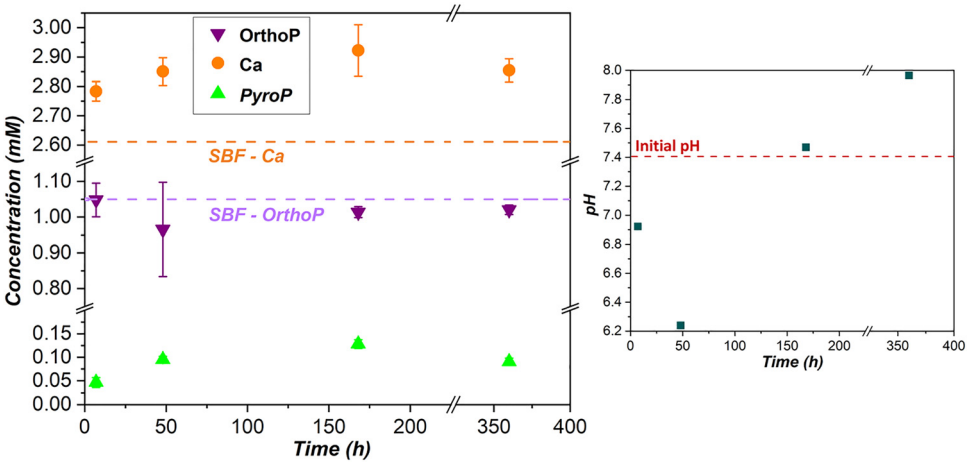

Fig. 7 Evolution of SBF solution as function of the duration of a-CPPc immersion (7 h, 48 h, 7 and 15 days). (Left) Concentration of calcium, orthophosphate (OrthoP) and pyrophosphate (PyroP) ions in SBF solution. The initial calcium and orthophosphate (OrthoP) ions concentrations are shown by the parallel doted lines (2.6 mM and 1.0 mM respectively). (Right) Evolution of the pH, initial pH of the SBF solution was around 7.4 (see red dotted line).

orthophosphate ions is stable and remains close to the initial value (1.0 mM) in SBF with a peak concentration at 1.02 mM.

3.2.2 Evolution in TRIS and TRIS + ALP. XRD analyses of a-CPPc cement after immersion in TRIS or TRIS + ALP media illustrate the evolution of the amorphous phase towards two crystalline phases after two days of immersion in the TRIS medium, *m*-CPPT-β ($Ca_2P_2O_7{\cdot}4H_2O$) and *m*-CPPD ($Ca_2P_2O_7{\cdot}2H_2O$). In the presence of ALP enzymes (in TRIS + ALP medium) the partial crystallization of a-CPPc cement appears more pronounced at day 2 and *m*-CPPD phase is favored, particularly after 6 days of immersion in TRIS + ALP.

The a-CPPc cement disk remaining mass follow-up after immersion in TRIS or TRIS + ALP during 2 and 6 days and photographs of a-CPPc cement before and after 6 days of immersion in TRIS or TRIS + ALP are presented in Fig. 9A and B, respectively.

In the TRIS medium, an increase in disk mass is observed after 2 days of immersion, probably associated with insufficient drying of materials after the evolution test, followed by a low decrease of approximately 3% at day 6. In the case of TRIS + ALP medium, there was an important variability of the mass values mainly due to partial disintegration of the cement disk in presence of ALP enzyme contributing in the variability of these measurements especially at day 2. That is the main reason why the differences between the TRIS + ALP mass data at day 2 and 6 cannot be considered as significant even if a mass loss may be associated with the transformation/crystallization of a-CPP into *m*-CPPD crystalline phase in the cement sample as identified by XRD analysis (Fig. 8). In addition, photographs of the a-CPPc disks (Fig. 9B) before and after 6 days of immersion in the TRIS or TRIS + ALP medium demonstrate the influence of ALP enzyme activity on the cement sample physical aspect and size. Indeed, after immersion in TRIS medium the global dimension of the cement disk remains the same even if a "shell" was observed around the disk also with some porosities. After immersion in the TRIS + ALP

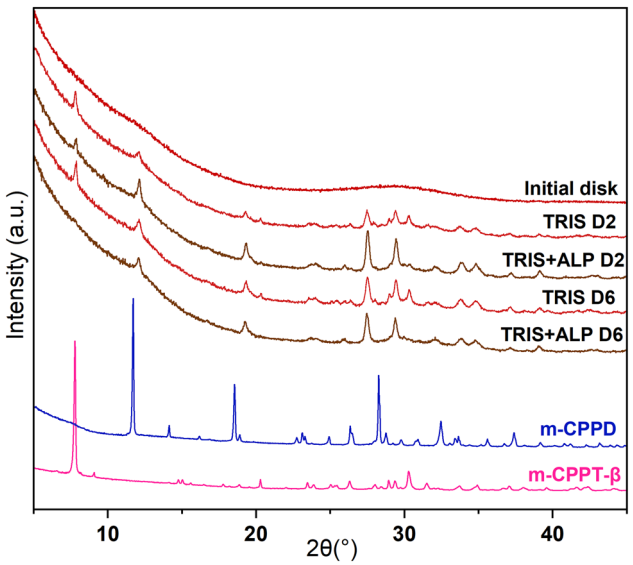

Fig. 8 XRD diffractograms of a-CPPc cement disk before (initial disk) and after immersion during 2 and 6 days in TRIS or TRIS + ALP solution.

medium the disk surface was visibly degraded/eroded by the action of the enzymes, which is evidenced by the presence of some cement particles next to the disk (Fig. 9B) and the decrease of disk diameter down to 0.75 cm.

After immersion in the TRIS medium, SEM observations made on the center of the pellet or on the "shell" are illustrated in Fig. 10. After two days, the center of the pellet consists of crystals in the form of thin platelets that may correspond to the characteristic morphology of the *m*-CPPT-β phase. At D6, a needle-like crystals morphology characteristic of the *m*-CPPD phase is evident. On the "shell," after two days, the observation of *m*-CPPT-β crystals in the form of platelets indicates greater crystallization. After six days, crystals corresponding to both the *m*-CPPT-β phase (platelets) and the

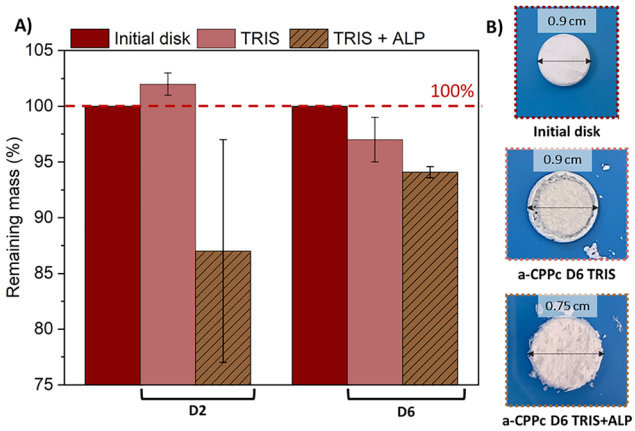

Fig. 9 (A) a-CPPc cement disks remaining mass (in triplicate), expressed as a percentage of mass remaining relative to mass before immersion, of a-CPPc cement after 2 and 6 days of immersion in TRIS medium with (TRIS + ALP) or without (TRIS) ALP enzymes. (B) Photographs of a-CPPc disks before and after 6 days of immersion in TRIS or TRIS + ALP medium.

m-CPPD phase (needles) are observed, which is consistent with the XRD results.

After 2 and 6 days of immersion in the TRIS + ALP medium, the a-CPPc cements exhibit a surface including smaller and less defined particles (than those observed in TRIS) which are characteristic of an amorphous phase; some needle-like crystals characteristic of the *m*-CPPD phase are also observed (Fig. 11). In agreement with XRD results (Fig. 8), in the presence of enzymes (TRIS + ALP), the m-CPPT-β phase (platelet-like crystals) no longer appears to be present on the sample surface.

After 6 days of immersion of the cements in the TRIS medium, the pH increased to a maximum of 9.2 whereas in the presence of enzymes (TRIS + ALP medium) the final pH measured is lower (around 8.6).

Fig. 12 shows the concentration of calcium, orthophosphate, and pyrophosphate ions titrated in TRIS and TRIS + ALP medium after a-CPPc cement immersion. In the TRIS medium, the measured ion concentration is close to 0.10 mM for each type of ion. A decrease in the concentration of pyrophosphate and calcium ions can be observed in the TRIS medium after immersion of a-CPPc cement for 2 and 6 days. In fact, the orthophosphate ion concentration decreases from 0.10 mM to 0.08 mM and the calcium ion concentration from 0.11 mM to 0.09 mM, which is consistent with the precipitation of *m*-CPPD and/or *m*-CPPT-β phases, both with a Ca/P equal to 1 and identified by XRD and SEM. In the TRIS + ALP medium, the presence of pyrophosphate ions is not detectable in the medium (< 0.02 μM), whereas orthophosphate ions concentration is much higher than in the TRIS medium (without enzyme) with a maximum concentration of 0.91 mM. These observations confirm that ALP enzyme activity induces the hydrolysis of pyrophosphate ions into orthophosphate ions.

3.3 Cytotoxicity and cytocompatibility of a-CPPc cement

Fig. 13A shows the cytotoxicity assessment of a-CPPc cements prepared with a liquid phase containing 2.5% w/w $K_4P_2O_7$

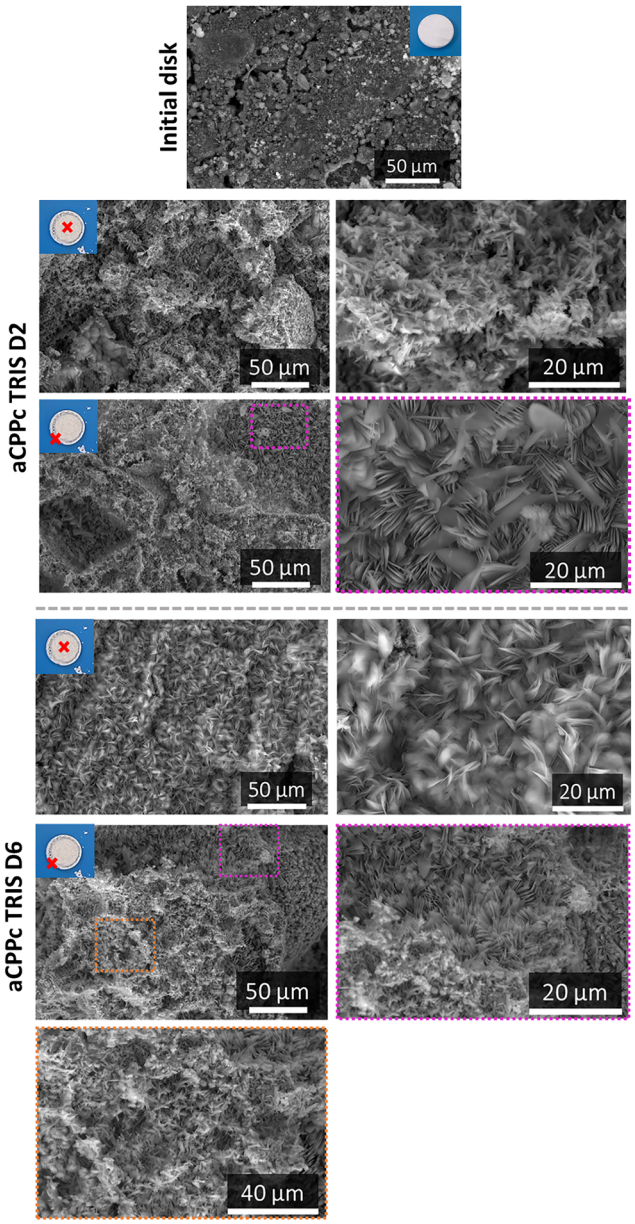

Fig. 10 SEM images of a-CPPc cement before and after 2 and 6 days of immersion in TRIS solution. Images have been taken on the center or the "shell" of the a-CPPc cement disks, the area of interest is marked by a red cross on the picture presented at the top left side of the corresponding micrograph.

(right) or 5% w/w $K_4P_2O_7$ (left). The 100% extract of the formulation prepared with 2.5% w/w $K_4P_2O_7$ is at the threshold of cytotoxicity, while the 5% w/w $K_4P_2O_7$ formulation is cytotoxic at 10%. Our hypothesis is that the proportion of potassium ions incorporated into the cement paste *via* the liquid phase including 2.5% or 5% w/w $K_4P_2O_7$, could be a crucial parameter for the cement's biological properties. Therefore, to go further, potassium ions were titrated in two extracts (the least and most diluted extracts were selected: 100% and 1% extracts, respectively) from a-CPPc samples including 5% or 2.5% w/w $K_4P_2O_7$ in the liquid phase (Fig. 13B). The concentration of

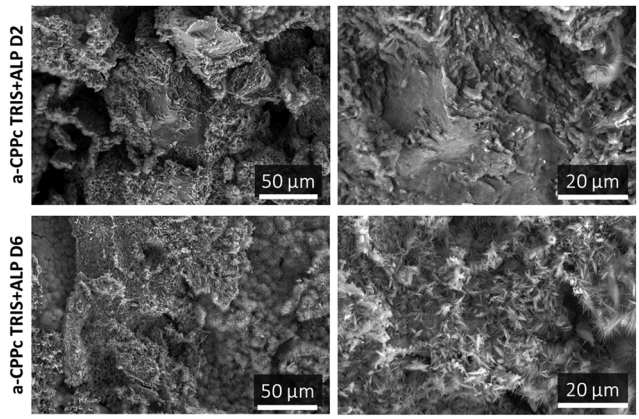

Fig. 11 SEM images of a-CPPc cement after 2 and 6 days of immersion in TRIS + ALP medium.

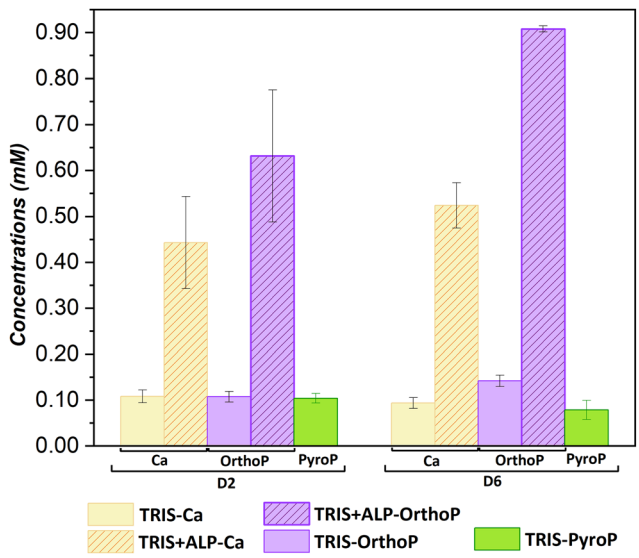

Fig. 12 Concentration of calcium, orthophosphate (OrthoP), and pyrophosphate (PyroP) ions in TRIS medium with (TRIS + ALP) and without (TRIS) ALP enzymes after 2 (D2) and 6 days (D6) of a-CPPc cement immersion. In the presence of ALP enzymes (TRIS + ALP), the concentration of pyrophosphate ions could not be measured because it was below the detection limit of the assay kit used (< 0.02 µM).

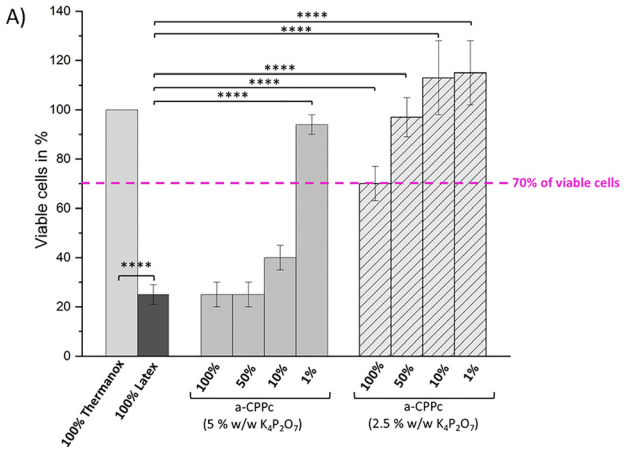

B)

Samples	Extract concentration (%)	Potassium ions concentration (ppm)	
		Extract *	Supernatant **
a-CPPc (5 % w/w $K_4P_2O_7$)	1	293 ± 3	299 ± 3
	100	6088 ± 82	5714 ± 77
a-CPPc (2.5 % w/w $K_4P_2O_7$)	1	234 ± 7	238 ± 7
	100	1100 ± 11	1131 ± 11
Medium before assays (EMEM + 10 % v/v serum)	-	200	

* **Extract:** medium after contact with cements, diluted (1%) or not (100%) with EMEM + 10 % v/v serum
** **Supernatant:** medium after cells were cultured in presence of extract

Fig. 13 (A) MTT assay for the evaluation of the cytotoxicity of a-CPPc cements prepared with a liquid phase containing 2.5% w/w $K_4P_2O_7$ (right) or 5% w/w $K_4P_2O_7$ (left): viability of L929 cells (clone NCTC 929, CCL1 (ATCC)), a murine fibroblast cell line, exposed to cement extracts obtained after 48 hours of contact with serum-free culture medium. Thermanox is the negative control and latex is the positive control for cytotoxicity. A cement is considered non-cytotoxic if the percentage of viable cells is equal to or greater than 70% compared to the negative control. ****$p <$ 0.0001 for the difference between the cements and the positive control, and between the positive and negative controls (one-way ANOVA, GraphPadPrism). (B) Concentration of potassium ions measured in undiluted (100%) and 1% diluted extracts and supernatant related to the MTT assay of a-CPPc cements and the medium before assays.

potassium ions measured in extracts in contact with the two a-CPPc cement formulations and diluted to 1% is between 230 and 300 ppm, and both samples were found to be non-cytotoxic (Fig. 13A). The pure extract (100%) in contact with a-CPPc cement at 5% w/w $K_4P_2O_7$ is cytotoxic (Fig. 13A) and the potassium concentration is around 6000 ppm (Fig. 13B). This is about six times higher than for the 100% extract of the a-CPPc formulation with 2.5% w/w $K_4P_2O_7$, which has been found to be at the limit of cytotoxicity. These results indicate that above 1000 ppm, the potassium concentration in the medium could contribute to the cytotoxicity of the a-CPPc cements. Finally, the potassium concentrations measured in the extracts and in the supernatants (medium after the extract has been in contact with the cells) displays a difference of less than 8%, therefore we can consider that the presence of cells did not alter the potassium concentration in the medium.

XRD and SEM characterization of the two types of a-CPPc cement (prepared with 2.5% or 5% w/w of $K_4P_2O_7$ in the liquid phase) after 48 h of immersion in EMEM serum free medium are presented in Fig. 14 and Fig. S8. SEM images illustrate the presence of needle-shaped crystals of varying size on the surface of the cement disks, identified as *m*-CPPD by XRD. Using a higher concentration of $K_4P_2O_7$ in the liquid phase led to a significant crystallization of a-CPPc samples, which amorphous halo on XRD patterns is less noticeable compared to the a-CPPc prepared with 2.5% w/w of $K_4P_2O_7$. Raman spectroscopy analyses (Fig. S9) are consistent with SEM and XRD observations and reveal that a-CPPc containing 5% w/w of $K_4P_2O_7$ is fully transformed into *m*-CPPD crystalline phase.

Furthermore, *m*-CPPD crystals formed during the evolution of a-CPPc in EMEM medium (Fig. 14) shows variations in peak relative intensity at 2θ of 27.3° and 29.3° on the XRD pattern, in comparison to the *m*-CPPD reference pattern (ICDD: COD 2107462). These observations have previously been confirmed

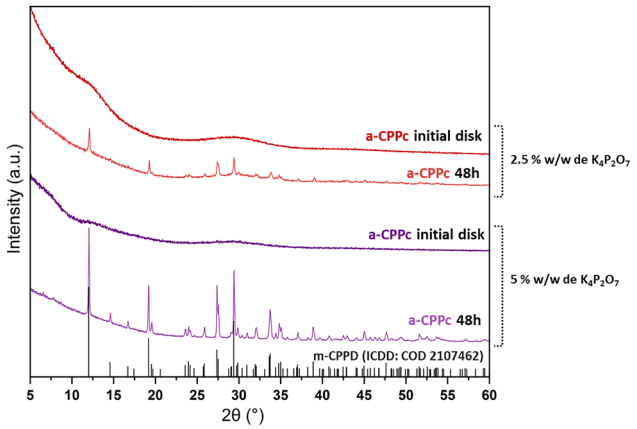

Fig. 14 X-ray diffractograms of a-CPPc cements prepared with a liquid phase containing 2.5% w/w $K_4P_2O_7$ (top) or 5% w/w $K_4P_2O_7$ (bottom), before and after 48 hours of immersion in EMEM serum-free medium. The *m*-CPPD reference X-ray diffraction pattern is also presented (ICDD: COD 2107462).

for agglomerated *m*-CPPDc crystals obtained by the cement route.[18] It suggests that crystallization mechanisms of a-CPP to *m*-CPPD inhibits or promotes crystal growth in specific directions.

3.4 Discussion on the *in vitro* physico-chemical and biological properties of a-CPPc cements

The acellular *in vitro* study of a-CPPc in aqueous medium highlighted the chemical reactivity of a-CPPc cement, which tends to crystallize in some conditions (in presence of ALP enzymes or in culture medium in absence of cells) into more stable crystalline phases such as *m*-CPPD and *m*-CPPT-β. In addition, the a-CPPc material exhibits an ability to release bioactive ions such as calcium and orthophosphate ions in the presence or not of ALP enzyme.

In the SBF solution, a-CPPc cement releases calcium and pyrophosphate ions, but the measured orthophosphate ion concentration is close to that initially present in the SBF. Furthermore, a higher proportion of orthophosphate ions was detected by Raman spectroscopy in the a-CPPc materials after 15 days of immersion in SBF. The presence of these ions in a-CPPc (demonstrated also by ^{1}H NMR and chemical titration) participates in stabilization of the amorphous structure and may explain why the release of orthophosphate ions into medium is very low. We did not observe apatite precipitation on the surface of the a-CPPc cement immersed in SBF. In previous work carried out under similar conditions on *m*-CPPD-based novel cement formulation, apatite formation was not observed on the surface of this cement too.[18] That can be explained by the potential of pyrophosphate ions to inhibit apatite crystallization as mentioned by several authors.[19,21,44] In addition, the pyrophosphate ion concentrations measured in the medium in contact with a-CPPc cement are up to nearly 10 times higher than those for *m*-CPPD cement reported in the literature demonstrating the *in vitro* bioactivity of this original a-CPPc amorphous cement formulation.[18]

In TRIS medium, with or without ALP enzyme, a-CPPc cement releases orthophosphate ions in addition to calcium and pyrophosphate ions. The differences observed in the ion release mechanism between SBF and TRIS media (with or without enzyme) can be explained by the effect of the presence of inorganic ions (Ca^{2+}, HPO_4^{2-}) in the former medium. It would be interesting to determine whether the supersaturation necessary for apatite precipitation was achieved in these different media.

In the presence of ALP enzyme, pyrophosphate ions are not detectable in the aqueous solution, whereas the orthophosphate ion concentration is much higher than that for the test in TRIS medium without enzyme (TRIS). After 6 days, the orthophosphate ion concentration in the a-CPPc cement filtrate is more than six times higher in the presence of ALP, with a maximum of 0.91 mM. These observations confirm that ALP enzyme activity induces the hydrolysis of pyrophosphate ions into orthophosphate ions. Compared to an apatite cement studied under the same experimental conditions,[18] the maximum orthophosphate ion concentration measured in the TRIS medium is twice as high for apatite. However, in the presence of ALP enzyme, the orthophosphate concentration measured in the a-CPPc cement filtrate is at least twice as high as that in contact with apatite or *m*-CPPD cement demonstrating the higher bioactivity of the present original amorphous calcium pyrophosphate cement. Similarly, the concentration of calcium ions released into the TRIS medium, with or without ALP enzyme, is much higher for a-CPPc cements than for apatite cement.[18] Altogether these results highlight the decisive advantages of obtaining such an amorphous calcium phosphate cement for bone applications. It should be noted that the hydrolysis of pyrophosphate ions according to eqn (1) and (2) can occur through various mechanisms discussed in the literature, namely direct hydrolysis of pyrophosphate ions in the medium by the ALP enzyme, which can be favored by the temperature of the medium (37 °C).[9] But also, direct hydrolysis by enzymes on the surface of materials, leading to their partial degradation, as shown in the photographs in Fig. 9B.[50]

In vitro cell tests carried out on a-CPPc point that this cement is non-cytotoxic when prepared with 2.5% w/w $K_4P_2O_7$, unlike *m*-CPPD cement, whose cytotoxicity was also assessed by a direct method.[18] However, by increasing the potassium ion concentration in the liquid phase to 5% w/w $K_4P_2O_7$, a cytotoxic response of cells is observed (Fig. 13A). Our results (Fig. 13a and B) showed that this cellular response could be correlated with the concentration of K^+ ions present in the medium after contact with the a-CPPc cements. Indeed, when the potassium concentration measured in the medium exceeds 1000 ppm (equivalent to 25.6 mmol L^{-1}), a cytotoxic response is observed in our experiment. Cell potassium homeostasis is known to be critical for cell viability.[51,52] For instance, hyperkaliemia results in persistent depolarization of cell membranes, leading to inactivation of sodium channels and impaired excitability.[53] In human body, hyperkalemia is defined as serum potassium level higher than 5.0 mmol L^{-1}. The mechanism by which the extracellular

potassium in our experiment would impair cell survival should be investigated.

In addition, the concentration of potassium released in extracts and supernatant related to the MTT assay correlates with the results of acellular tests. Indeed, the latter reflect the high reactivity of a-CPPc cement in all media, evolving towards more stable crystalline phases, such as *m*-CPPD, and releasing higher concentrations of calcium ions, pyrophosphate and orthophosphate ions compared to other calcium (pyro)-phosphate-based cement formulations.[18] Finally, the K^+ ion concentration incorporated into the cement formulation also appears to influence the chemical stability of the a-CPP phase. Formulation with 2.5% w/w $K_4P_2O_7$ retains an amorphous phase, while the 5% w/w $K_4P_2O_7$ formulation seems to be fully transformed into *m*-CPPD.

4. Conclusion

This study aimed to develop an amorphous calcium pyrophosphate cement. The mixture of a solid phase constituted of a thermally activated a-CPP and an aqueous solution containing 2.5% or 5% w/w of $K_4P_2O_7$ results, after 24 hours of maturation in a wet atmosphere at 37 °C, in an amorphous, hard, and cohesive cement. The initial setting time is 22 ± 2 minutes. Thermogravimetric analysis of a-CPPc confirms the presence in a-CPPc of an amorphous phase of hydrated calcium pyrophosphate including in average n = 2.72 water molecules per $Ca_2P_2O_7$ unit. The chemical setting reaction follow-up showed that this amorphous phase is stable for up to 48 hours of maturation time, after which the cement paste partially crystallizes into a calcium pyrophosphate dihydrate, *m*-CPPD ($Ca_2P_2O_7{\cdot}2H_2O$) phase. This phenomenon has been linked to the similarity in the number of structural water molecules between a-CPPc and the *m*-CPPD phase. The amount of structural water associated with the a-CPP act reagent also appears to influence the stability of the a-CPP phase, with a higher number of water molecules stabilizing the amorphous phase in a-CPP paste over time. The characterization of the various amorphous calcium pyrophosphate phases involved in this cement route (a-CPP, a-CPP act, and a-CPPc) using ^1H and ^1H–^{31}P NMR spectroscopy indicates that synthesis protocol of the a-CPP reagent influences the organization of the water molecules in synthesized a-CPP, which then has an impact on the a-CPP act and a-CPPc samples obtained. ^1H–^{31}P NMR and chemical analysis of the thermally activated a-CPP and the corresponding cement revealed the presence of orthophosphate ions, contributing in the stabilization of the amorphous calcium pyrophosphate. The thermal activation of a-CPP phase contributes to its stabilization by forming orthophosphate ions, conversely, the loss of structural water molecules associated with this amorphous phase contributes to its reactivity. Indeed, the latter confers some bioactivity to this a-CPPc cement, resulting in a significant release of calcium and orthophosphates ions, which are known to be essential for bone apatite formation. The action of the ALP enzyme induces twice as much release of these bioactive ions from a-CPPc cement as from a biomimetic apatite-based cement or other crystalline calcium pyrophosphate formulations, such as *m*-CPPD cement. The *in vitro* cytotoxicity results showed that a-CPPc cement is non-cytotoxic when prepared with a liquid phase with the lowest potassium ions concentration tested, the latter being a key parameter of cement formulation for its biological properties as demonstrated by chemical titration. These *in vitro* physicochemical and biological results on this intrinsically bioactive and biologically responsive original and fully amorphous hydrated calcium pyrophosphate cement formulation paves the way to widen the family of bioactive calcium phosphate cements for bone reconstruction. The transformation of the amorphous phase into a more stable crystalline phases also opens up interesting prospects. Indeed, the hydrolysis of crystalline calcium pyrophosphate phases (*m*-CPPD, *t*-CPPD) could lead to the formation of brushite, which can itself be hydrolyzed into hydroxyapatite.

Author contributions

L. Touati: physico-chemical investigation, formal analysis, visualization, data curation, writing – original draft. M. Y. Hammami: solid state NMR investigation, formal analysis, visualization. C. Damia: writing – review & editing. M. Renard: *in vitro* biocompatibility investigation, formal analysis. D. Bertrand: investigation by atomic absorption spectrometry. M. Durand: supervision of the *in vitro* biocompatibility study, resources. J. Amédée: conceptualization, methodology and supervision of the biocompatibility study, writing – review & editing. C. Bonhomme: conceptualization, methodology and supervision of the solid-state NMR analyses, writing – review & editing. C. Combes: conceptualization, methodology, supervision, writing – review & editing, funding acquisition.

Conflicts of interest

There are no conflicts to declare.

Data availability

The data supporting this article have been included as part of the supplementary information (SI). Supplementary information: Tables S1, S2 and Fig. S1–S9. Further experimental details and data are included in the PhD manuscript of Louize TOUATI (Université de Toulouse, France, 2025) which is publicly available at the following address (https://theses.fr/2025TLSEP130). Supporting information: further characterization results (FTIR/Raman/solid-state NMR spectroscopy, SEM, TGA, porosimetry) related to the synthesized reactive powders and cement paste before, during and after chemical setting are presented. Complementary characterization by Raman spectroscopy and SEM of cements after evolution in simulated body fluid or EMEM serum-free culture medium are also shown. See DOI: https://doi.org/10.1039/d5tb02873f.

Acknowledgements

This work was supported by the french Agence Nationale de Recherche (OASIS grant no. ANR-21-CE19-0031-02), the Institut Carnot Chimie Balard Cirimat (InterCarnot project 2021, supported through the ANR program no. 16 CARN 0008-01) and the Occitanie Region (PYRODIAG grant no. 00079351/21012581).

References

1 M. Bohner, Design of Ceramic-Based Cements and Putties for Bone Graft Substitution, *eCM*, 2010, **20**, 1–12, DOI: 10.22203/eCM.v020a01.

2 J. Zhang, W. Liu, V. Schnitzler, F. Tancret and J.-M. Bouler, Calcium Phosphate Cements for Bone Substitution: Chemistry, Handling and Mechanical Properties, *Acta Biomater.*, 2014, **10**(3), 1035–1049, DOI: 10.1016/j.actbio.2013.11.001.

3 A. Sugawara, K. Asaoka and S.-J. Ding, Calcium Phosphate-Based Cements: Clinical Needs and Recent Progress, *J. Mater. Chem. B*, 2013, **1**(8), 1081–1089.

4 S. Samavedi, A. R. Whittington and A. S. Goldstein, Calcium Phosphate Ceramics in Bone Tissue Engineering: A Review of Properties and Their Influence on Cell Behavior, *Acta Biomater.*, 2013, **9**(9), 8037–8045, DOI: 10.1016/j.actbio.2013.06.014.

5 X.-D. Li, D.-W. Yan, H.-H. Ren, Q.-Y. Zhang and Y.-G. Yan, Fabricating Biodegradable Calcium Phosphate/Calcium Sulfate Cement Reinforced with Cellulose: In Vitro and in Vivo Studies, *J. Mater. Chem. B*, 2023, **11**(2), 303–315, DOI: 10.1039/D2TB02191A.

6 E. Fernández, M. D. Vlad, M. Montserrat Gel, J. López, R. Torres, J. V. Cauich and M. Bohner, Modulation of porosity in apatitic cements by the use of alpha-tricalcium phosphate-calcium sulphate dihydrate mixtures, *Biomaterials*, 2005, **26**(17), 3395–3404, DOI: 10.1016/j.biomaterials.2004.09.023.

7 C. Combes, R. Bareille and C. Rey, Calcium Carbonate–Calcium Phosphate Mixed Cement Compositions for Bone Reconstruct'ion, *J. Biomed. Mater. Res.*, 2006, **79A**(2), 318–328, DOI: 10.1002/jbm.a.30795.

8 A. A. Mirtchi, J. Lemaître and E. Munting, Calcium Phosphate Cements: Study of the β-Tricalcium Phosphate—Dicalcium Phosphate—Calcite Cements, *Biomaterials*, 1990, **11**(2), 83–88, DOI: 10.1016/0142-9612(90)90121-6.

9 L. M. Grover, A. J. Wright, U. Gbureck, A. Bolarinwa, J. Song, Y. Liu, D. F. Farrar, G. Howling, J. Rose and J. E. Barralet, The Effect of Amorphous Pyrophosphate on Calcium Phosphate Cement Resorption and Bone Generation, *Biomaterials*, 2013, **34**(28), 6631–6637, DOI: 10.1016/j.biomaterials.2013.05.001.

10 M. H. Alkhraisat, F. T. Mariño, C. R. Rodríguez, L. B. Jerez and E. L. Cabarcos, Combined Effect of Strontium and Pyrophosphate on the Properties of Brushite Cements, *Acta Biomater.*, 2008, **4**(3), 664–670, DOI: 10.1016/j.actbio.2007.12.001.

11 A. A. Mirtchi, J. Lemaître and E. Hunting, Calcium Phosphate Cements: Action of Setting Regulators on the Properties of the β-Tricalcium Phosphate-Monocalcium Phosphate Cements, *Biomaterials*, 1989, **10**(9), 634–638, DOI: 10.1016/0142-9612(89)90120-8.

12 R. A. Perez, H. W. Kim and M. P. Ginebra, Polymeric Additives to Enhance the Functional Properties of Calcium Phosphate Cements, *J. Tissue Eng.*, 2012, **3**(1), 2041731412439555, DOI: 10.1177/2041731412439555.

13 J. H. Lee, D. H. Lee, H. S. Ryu, B.-S. Chang, K. S. Hong and C. K. Lee, Porous Beta-Calcium Pyrophosphate as a Bone Graft Substitute in a Canine Bone Defect Model, *KEM*, 2003, **240–242**, 399–402, DOI: 10.4028/www.scientific.net/KEM.240-242.399.

14 S. Koo, B. König, S. Allegrini, M. Yoshimoto, M. J. Carbonari and F. F. Mitri-Luiz, Titanium Implant Osseointegration with Calcium Pyrophosphate in Rabbits, *J. Biomed. Mater. Res.*, 2006, **76B**(2), 373–380, DOI: 10.1002/jbm.b.30383.

15 J. H. Lee, B.-S. Chang, U.-O. Jeung, K.-W. Park, M.-S. Kim and C.-K. Lee, The First Clinical Trial of Beta-Calcium Pyrophosphate as a Novel Bone Graft Extender in Instrumented Posterolateral Lumbar Fusion, *Clin. Orthop. Surg.*, 2011, **3**(3), 238, DOI: 10.4055/cios.2011.3.3.238.

16 B.-H. Lee, M.-H. Hong, M.-C. Kim, J.-S. Kwon, Y.-M. Ko, H.-J. Choi and Y.-K. Lee, Bone Cement with a Modified Polyphosphate Network Structure Stimulates Hard Tissue Regeneration, *J. Biomater. Appl.*, 2016, **31**(3), 344–356, DOI: 10.1177/0885328216664239.

17 F. Darvishnia, S. M. Rabiee and D. Sabour, Bioactivity Evaluation of Printable Calcium Polyphosphate/Alginoplast Cement for Bone Tissue Engineering; In Vitro Study, *Bioprinting*, 2022, **27**, e00210, DOI: 10.1016/j.bprint.2022.e00210.

18 L. Touati, C. Leroy, C. Damia, M. Renard, O. Marsan, M. Durand, H. K. Ea, J. Amédée and C. Combes, Formulation, *in Vitro* Physico-Chemical and Biological Assessment of Calcium Pyrophosphate Dihydrate Cement for Bone Tissue Engineering, *Acta Biomater.*, 2025, **206**, 420–433, DOI: 10.1016/j.actbio.2025.09.022.

19 H. Fleisch and S. Bisaz, Mechanism of Calcification: Inhibitory Role of Pyrophosphate, *Nature*, 1962, **195**(4844), 911, DOI: 10.1038/195911a0.

20 H. Fleisch, J. Maerki and R. G. G. Russell, Effect of Pyrophosphate on Dissolution of Hydroxyapatite and Its Possible Importance in Calcium Homeostasis, *Exp. Biol. Med.*, 1966, **122**(2), 317–320, DOI: 10.3181/00379727-122-31123.

21 N. Eidelman, W. E. Brown and J. L. Meyer, The Effect of Pyrophosphate Concentrations on Calcium Phosphate Growth on Well-Crystallized Octacalcium Phosphate and Hydroxyapatite Seed Crystals, *J. Crystal Growth*, 1991, **108**(1–2), 385–393, DOI: 10.1016/0022-0248(91)90386-J.

22 L. Degli Esposti and M. Iafisco, Amorphous Calcium Phosphate, the Lack of Order Is an Abundance of Possibilities, *Biomater. Biosyst.*, 2022, **5**, 100037, DOI: 10.1016/j.bbiosy.2021.100037.

23 C. Combes and C. Rey, Amorphous Calcium Phosphates: Synthesis, Properties and Uses in Biomaterials, *Acta Biomater.*, 2010, **6**(9), 3362–3378, DOI: 10.1016/j.actbio.2010.02.017.

24 S. Allegrini Jr, A. C. da Silva, M. Tsujita, M. B. Salles, S. A. Gehrke and F. J. C. Braga, Amorphous Calcium

Phosphate (ACP) in Tissue Repair Process, *Microsc. Res. Tech.*, 2018, **81**(6), 579–589, DOI: 10.1002/jemt.23013.

25 R. Gelli, F. Ridi and P. Baglioni, The Importance of Being Amorphous: Calcium and Magnesium Phosphates in the Human Body, *Adv. Colloid Interface Sci.*, 2019, **269**, 219–235, DOI: 10.1016/j.cis.2019.04.011.

26 C. Slater, D. Laurencin, V. Burnell, M. E. Smith, L. M. Grover, J. A. Hriljac and A. J. Wright, Enhanced Stability and Local Structure in Biologically Relevant Amorphous Materials Containing Pyrophosphate, *J. Mater. Chem.*, 2011, **21**(46), 18783, DOI: 10.1039/c1jm13930d.

27 P. Gras, C. Rey, O. Marsan, S. Sarda and C. Combes, Synthesis and Characterisation of Hydrated Calcium Pyrophosphate Phases of Biological Interest, *Eur. J. Inorg. Chem.*, 2013, **2013**(34), 5886–5895, DOI: 10.1002/ejic.201300955.

28 J. Soulié, P. Gras, O. Marsan, D. Laurencin, C. Rey and C. Combes, Development of a New Family of Monolithic Calcium (Pyro)Phosphate Glasses by Soft Chemistry, *Acta Biomater.*, 2016, **41**, 320–327, DOI: 10.1016/j.actbio.2016.05.030.

29 M. Desbord, J. Soulié, C. Rey and C. Combes, Tunable Behavior in Solution of Amorphous Calcium Ortho/Pyrophosphate Materials: An Acellular In Vitro Study, *ACS Biomater. Sci. Eng.*, 2022, **8**(6), 2363–2374, DOI: 10.1021/acsbiomaterials.1c01618.

30 C. Feng, B.-Q. Lu, Y. Fan, H. Ni, Y. Zhao, S. Tan, Z. Zhou, L. Liu, J. A. Hachtel, D. Kepaptsoglou, B. Wu, D. Gebauer, S. He and F. Chen, Amorphous 1-D Nanowires of Calcium Phosphate/Pyrophosphate: A Demonstration of Oriented Self-Growth of Amorphous Minerals, *J. Colloid Interface Sci.*, 2024, **657**, 960–970, DOI: 10.1016/j.jcis.2023.12.002.

31 A. L. Boskey and A. S. Posner, Conversion of Amorphous Calcium Phosphate to Microcrystalline Hydroxyapatite. A pH-Dependent, Solution-Mediated, Solid-Solid Conversion, *J. Phys. Chem.*, 1973, **77**(19), 2313–2317, DOI: 10.1021/j100638a011.

32 S. Somrani, M. Banu, M. Jemal and C. Rey, Physico-Chemical and Thermochemical Studies of the Hydrolytic Conversion of Amorphous Tricalcium Phosphate into Apatite, *J. Solid State Chem.*, 2005, **178**(5), 1337–1348, DOI: 10.1016/j.jssc.2004.11.029.

33 A. Dey, P. H. H. Bomans, F. A. Müller, J. Will, P. M. Frederik, G. De With and N. A. J. M. Sommerdijk, The Role of Prenucleation Clusters in Surface-Induced Calcium Phosphate Crystallization, *Nat. Mater.*, 2010, **9**(12), 1010–1014, DOI: 10.1038/nmat2900.

34 M. Kazanci, P. Fratzl, K. Klaushofer and E. P. Paschalis, Complementary Information on In Vitro Conversion of Amorphous (Precursor) Calcium Phosphate to Hydroxyapatite from Raman Microspectroscopy and Wide-Angle X-Ray Scattering, *Calcif. Tissue Int.*, 2006, **79**(5), 354–359, DOI: 10.1007/s00223-006-0011-9.

35 A. Lotsari, A. K. Rajasekharan, M. Halvarsson and M. Andersson, Transformation of Amorphous Calcium Phosphate to Bone-like Apatite, *Nat. Commun.*, 2018, **9**(1), 4170, DOI: 10.1038/s41467-018-06570-x.

36 P. Gras, A. Baker, C. Combes, C. Rey, S. Sarda, A. J. Wright, M. E. Smith, J. V. Hanna, C. Gervais, D. Laurencin and C. Bonhomme, From Crystalline to Amorphous Calcium Pyrophosphates: A Solid State Nuclear Magnetic Resonance Perspective, *Acta Biomater.*, 2016, **31**, 348–357, DOI: 10.1016/j.actbio.2015.10.016.

37 S. Omelon, J. Georgiou, Z. J. Henneman, L. M. Wise, B. Sukhu, T. Hunt, C. Wynnyckyj, D. Holmyard, R. Bielecki and M. D. Grynpas, Control of Vertebrate Skeletal Mineralization by Polyphosphates, *PLoS One*, 2009, **4**(5), e5634, DOI: 10.1371/journal.pone.0005634.

38 H. Flodgaard and P. Fleron, Thermodynamic Parameters for the Hydrolysis of Inorganic Pyrophosphate at pH 7.4 as a Function of $[Mg^{2+}]$, $[K^{+}]$, and Ionic Strength Determined from Equilibrium Studies of the Reaction, *J. Biol. Chem.*, 1974, **249**(11), 3465–3474, DOI: 10.1016/S0021-9258(19)42596-9.

39 I. A. Silver, R. J. Murrills and D. J. Etherington, Microelectrode Studies on the Acid Microenvironment beneath Adherent Macrophages and Osteoclasts, *Exp. Cell Res.*, 1988, **175**(2), 266–276, DOI: 10.1016/0014-4827(88)90191-7.

40 Y. Xu, T. F. Cruz and K. P. Pritzker, Alkaline Phosphatase Dissolves Calcium Pyrophosphate Dihydrate Crystals, *J. Rheumatol.*, 1991, **18**(10), 1606–1610.

41 M. Yang, X. Cai, C. Wang, Z. Wang, F. Xue, C. Chu, J. Bai, Q. Liu and X. Ni, Highly Stable Amorphous (Pyro)-Phosphate Aggregates: Pyrophosphate as a Carrier for Bioactive Ions and Drugs in Bone Repair Applications, *ACS Omega*, 2024, **9**(22), 23724–23740, DOI: 10.1021/acsomega.4c01660.

42 B. M. Fung, A. K. Khitrin and K. Ermolaev, An Improved Broadband Decoupling Sequence for Liquid Crystals and Solids, *J. Magn. Reson.*, 2000, **142**(1), 97–101, DOI: 10.1006/jmre.1999.1896.

43 T. Mosmann, Rapid Colorimetric Assay for Cellular Growth and Survival: Application to Proliferation and Cytotoxicity Assays, *J. Immunol. Methods*, 1983, **65**(1), 55–63, DOI: 10.1016/0022-1759(83)90303-4.

44 P. T. Cheng and K. P. Pritzker, Pyrophosphate, Phosphate Ion Interaction: Effects on Calcium Pyrophosphate and Calcium Hydroxyapatite Crystal Formation in Aqueous Solutions, *J. Rheumatol.*, 1983, **10**(5), 769–777.

45 F. Babonneau, C. Bonhomme, S. Hayakawa and A. Osaka, Solid State NMR Characterization of Nano-Crystalline Hydroxy-Carbonate Apatite Using 1H-31P-13C Triple Resonance Experiments, *MRS Proc.*, 2006, **984**, 0984-MM06-05, DOI: 10.1557/PROC-984-0984-MM06-05.

46 A. Nommeots-Nomm, L. Hupa, D. Rohanová and D. S. Brauer, A Review of Acellular Immersion Tests on Bioactive Glasses––Influence of Medium on Ion Release and Apatite Formation, *Int. J. Appl. Glass Sci.*, 2020, **11**(3), 537–551, DOI: 10.1111/ijag.15006.

47 P. Gras, Etude Physico-Chimique et Structurale de Pyrophosphate de Calcium Hydratés: Application Aux Micro-Calcifications Associées à La Maladie de l'arthrose, PhD thesis, INP Toulouse, 2014.

48 I. Cuesta Mayorga, J. Astilleros and L. Fernández-Díaz, Precipitation of $CaCO_3$ Polymorphs from Aqueous Solutions: The Role of pH and Sulphate Groups, *Minerals*, 2019, **9**(3), 178, DOI: 10.3390/min9030178.

49 H. Du and E. Amstad, Water: How Does It Influence the $CaCO_3$ Formation?, *Angew. Chem., Int. Ed.*, 2020, **59**(5), 1798–1816, DOI: 10.1002/anie.201903662.

50 T. Shinozaki, Y. Xu, T. F. Cruz and K. P. Pritzker, Calcium Pyrophosphate Dihydrate (CPPD) Crystal Dissolution by Alkaline Phosphatase: Interaction of Alkaline Phosphatase on CPPD Crystals, *J. Rheumatol.*, 1995, **22**(1), 117–123.

51 B. F. Palmer and D. J. Clegg, Physiology and Pathophysiology of Potassium Homeostasis: Core Curriculum 2019, *Am. J. Kidney Dis.*, 2019, **74**(5), 682–695, DOI: 10.1053/j.ajkd.2019.03.427.

52 M. Warny and C. P. Kelly, Monocytic Cell Necrosis Is Mediated by Potassium Depletion and Caspase-like Proteases, *Am. J. Physiol.: Cell Physiol.*, 1999, **276**(3), C717–C724, DOI: 10.1152/ajpcell.1999.276.3.C717.

53 R. W. Hunter and M. A. Bailey, Hyperkalemia: Pathophysiology, Risk Factors and Consequences, *Nephrol., Dial., Transplant.*, 2019, **34**(Supplement_3), iii2–iii11, DOI: 10.1093/ndt/gfz206.